arXiv:1608.07615v2 [cond-mat.mtrl-sci] 15 Nov 2016

Grain-resolved kinetics and rotation during grain growth of nanocrystalline Aluminium by molecular dynamics

Paul W. Hoffrogge[a], Luis A. Barrales-Mora[a,*]

[a]*Institute of Physical Metallurgy and Metal Physics, RWTH Aachen University, D-52056 Aachen, Germany*

Abstract

Grain growth in nanocrystalline Al was studied by means of molecular dynamics simulations. The novelty of this study results from the utilization of an algorithm to resolve per-grain kinetics and orientation change from molecular dynamics data sets. To this aim, a highly efficient algorithm for the identification and reconstruction of crystallites from molecular dynamics data sets of FCC materials was developed. This method is capable of calculating specific attributes of grains, namely, volume, center of mass, average orientation and orientation spread. In addition, it provides a mapping method to track grains during time-row data sets. In the present contribution, we describe and validate the algorithm, which is then used to analyze grain growth in polycrystalline Al with a weak texture. For the conditions tested, the algorithm was able to find all of the input orientations and reconstruct the grains according to their crystallographic orientation. With the help of the developed algorithms, we studied grain growth kinetics and grain rotation. The results of the simulations showed slightly slowed-down kinetics in particular in the initial stages of grain growth and marginal rotation of the grains.

Keywords: Molecular-Dynamics, Grain Reconstruction, Post-processing, Parallelization, Grain Growth, Grain Rotation

*Corresponding author
Email address: barrales@imm.rwth-aachen.de (Luis A. Barrales-Mora)

1. Introduction

1.1. Grain growth in nanocrystalline polycrystals

Nanomaterials have become an important source for the development of new technologies due to their extraordinary properties that allow their application in fields where conventional materials fail. Among other important technological fields, nanomaterials have been utilized in medicine (drug delivery), electronics (circuit miniaturization), aerospace industry (improved fatigue-resistant materials) and many other applications. Nevertheless, due to the high density of crystal defects per unit volume in polycrystalline nanomaterials, they are in such a state of thermodynamic non-equilibrium that provides, even at room temperature, a tremendous driving force for the elimination of the crystal defects and thus, for the transition from nano- to micro-sized grained materials. Hence, the thermal stability of nanomaterials is of utmost importance for their design and development.

The thermal stability of nanocrystalline materials is still a scientific conundrum owing to the intrinsic difficulties of investigating opaque materials with nanoscaled grains and even smaller microstructural features. Nanomaterials are prone to microstructural change because they own a very high free energy ΔG stemming from their large density of crystal defects in particular grain boundaries. Nevertheless, a polycrystal is not exclusively composed of grain boundaries. The junctions that connect grain boundaries, namely triple lines and quadruple junctions, also form part of the polycrystalline structure and affect the microstructural evolution under certain conditions. For mesoscopic grain sizes, the volume occupied by grain boundaries exceeds by orders of magnitude that of other structural elements. However, this difference becomes insignificant in nano-sized materials as triple lines, being the most frequent topological element, can occupy as much volume as grain boundaries in a microstructure. The contribution of these components to the free energy is so high that most rapid grain growth is expected and also usually observed [1, 2, 3].

Different approaches have been suggested for the stabilization of the mi-

crostructure in nanomaterials [4, 5, 6]. There are basically two approaches to achieve thermal stability in nanocrystalline materials, namely, the *kinetic* and the *thermodynamic approach* [5]. In the former, it is sought to hinder grain boundaries by incorporating obstacles for their migration [7, 8, 9, 10, 11, 12, 13, 14, 15, 16, 17, 18, 19, 20, 21, 22, 23, 24]. In this context, there is also available literature that seems to suggest that intrinsic phenomena to the grain boundary structure might aid thermal stability during the normal development of the microstructure[25, 26, 27, 28, 29]. The second approach relies on the decrease of the free energy caused by the segregation of solute atoms to grain boundaries [30, 31, 32, 33].

1.2. Simulation of grain growth in nanocrystalline polycrystals

Different computer models have been utilized in the past to simulate grain growth in nanocrystalline materials. Most of these simulations have been performed by mesoscopic models [34, 35, 36, 37, 7, 8, 9, 38, 10, 11, 12, 39, 40, 41]. These models rely on the properties of the structural elements of a microstructure, namely, the grain boundaries, the triple lines and the quadruple junctions. Any effect acting on these elements can be separately incorporated to the models. The advantage of these models is that they allow the simulation of relatively large representative volume elements (RVE) that can be composed of thousand to million grains and thus, the RVEs are statistically representative. The disadvantage of mesoscopic models is that the effects and physical mechanisms are pre-defined and pre-implemented. This is useful to test theories by isolating particular effects that are expected to affect considerably the evolution of a system but for obvious reasons, it is impossible to resolve the mechanisms of phenomena acting at the atomic scale. Nevertheless, a combination with experiments or atomistic simulation is most useful to complement the models and/or understand particular aspects of the experiments.

By contrast, atomistic simulations allow the determination of the mechanisms of the phenomena involved. In the case, of molecular dynamics simulations empirical interatomic potentials are utilized to describe interatomic interactions

so far with great success. The disadvantages of atomistic simulations is that the volume that can be simulated in a reasonable time is very limited compared to mesoscopic simulations. This results occasionally in insufficient statistical representativeness and undesired effects of the size of the simulated volume. Regarding grain growth, molecular dynamics have been already employed to simulate grain growth. In particular, the seminal work by Farkas et al. [42, 43, 44, 45, 46, 47], Haslam and Yamakov [48, 49, 50], Holm and Foiles [27] and Srolovitz et al. [51, 26, 52, 53, 54] have substantially advanced our knowledge on the mechanisms of grain growth in nanocrystalline materials. The purpose of the present manuscript is to identify particular mechanisms of grain growth in nanocrystalline materials. For this purpose, we utilized molecular dynamics simulations and developed novel characterization methods for the evaluation of computational microstructures from molecular dynamics data sets.

1.3. Post-processing of molecular dynamics

In molecular dynamics (MD) simulations, the analysis and interpretation of the data remain a substantial and difficult part. Certain tools are required in order to reduce the amount of information and obtain useful quantities. In several situations, information on the evolution of 3D features is necessary, for example, grains in polycrystalline aggregates. This information is, however, not delivered by most of the available methods for the characterization of MD data sets. This task remains difficult because it involves identifying crystallographically the environment of the atoms to assign an orientation respective to a coordinate system and to reconstruct from this information the volume with identical orientation i.e., the grains. Due to the mathematical complexity of rotations and reconstruction algorithms, these calculations are slow and costly for their execution during runtime and even during post-processing if large data sets are involved. Nevertheless, several methods which enable the identification of crystal structures from atomic-based data have been already developed. The most straightforward way to distinguish between some of these is to compute the coordination number, i.e. the number of nearest neighbors (NNs) or next-

nearest neighbors (NNNs) of the atoms. While this is a fast tool and also easy to implement, it obviously cannot distinguish between different atomic structures exhibiting the same coordination number. Another technique which allows a much more reliable identification of crystalline structures was first introduced by Honeycutt and Andersen [55]. This method analyzes the extent and connectivity properties of atom-diagrams which are comprised of nearest neighbors to two adjacent atoms. Based on this principle, also known as Common Neighbor Analysis or CNA, several algorithms have been implemented [56, 57, 58] and successfully performed to MD simulation data. Similarly, the centro-symmetry parameter, energy filters, bond order and angle and Voronoi analysis can also be used to discriminate atoms arranged in specific crystal structures [56]. Nevertheless, none of these methods can distinguish between groups of atoms with the same crystallographic orientation. To differentiate between differently oriented crystals, the definition of order parameters has been utilized. The drawbacks of this approach are that the orientations ought to be known beforehand and that complex rotations of the crystals might out-range the scope of the parameter. Nevertheless, this approach has been successfully utilized in numerous simulations to track, for instance, grain boundaries [59, 52, 53, 60, 61] and grain rotation [62, 63, 64, 65, 66].

The motivation of the present contribution is to introduce a method that allows the determination of the relative orientation of groups of atoms and reconstruct the grain from only this information. The method is able to generate a space-resolved three dimensional grain decomposition of atom-position data sets for FCC materials, such as those generated by MD-simulations. The first step of the method calculates an orientation for each atom by taking into account the positions of the nearest-neighbor atoms. In a second step, the method generates grain entities from atoms with similar orientations by collecting them via nearest-neighbor paths. The method is capable of calculating grain specific properties, namely volume, center of mass, average orientation and orientation spread. The method additionally provides a mapping method in order to track grains during a time-row data set. The method is introduced in order to be able

to track the grain growth evolution of individual grains during MD-simulations, additionally enabling a grain-resolved visualization of polycrystalline FCC data sets. Whereas the algorithms here presented were independently developed, they are admittedly similar to the method introduced by Panzarino et al. [67, 68]. However, we emphasize that in contrast to these previous contributions, we developed our algorithms for high-performance post-processing and that we offer the code to the community as a totally open-source project [69].

2. Methods

To identify the grains from a data set containing atomic positions, it is necessary to determine first the orientation of the atoms as a per-atom attribute from the local neighborhood. Once an atom (referred to as *central atom*) is selected arbitrarily, the calculation of the orientation proceeds in the following way:

1. Identify all the nearest neighbors and calculate the relative positions of the neighbors to the corresponding central atom.
2. Determine the affine 3×3 transformation matrix M from the reference (non-rotated case) to the current crystal-configuration.
3. Determine the rotation that best fits M as a least square solution.

All of these steps have an inherent mathematical and/or programmatic complexity. In the present section, we will discuss the algorithms that were utilized to solve each of these problems. In the appendix, these solutions are presented in the form of pseudo-code whereas the program is offered as an open-source project [70].

2.1. Orientation determination

The calculation begins with the identification of the nearest-neighbors. Once the neighbors of an atom have been identified, displacement vectors are calculated with the current atom as origin. These vectors are then normalized so

that only unit vectors are used for the orientation calculation. Since in the FCC crystal structure each neighbor has an antipodal counterpart, the list of nearest neighbor vectors is reduced by finding vectors with a near 180°-relationship. The resulting mean direction $\vec{v_r}$ is calculated by vector subtraction of any $\vec{v}$ and its antipodal partner $\vec{v_a}$:

$$\vec{v_r} = \frac{1}{2}(\vec{v} - \vec{v_a}) \tag{1}$$

In the FCC lattice, there are three pairs of neighbor vectors, each lying on different {100} planes. Since each vector ought to have only one defined perpendicular partner in the FCC-case, we try to find the directions of this planes by identifying vector pairs with a near 90°-relationship. Now, at least six different vectors must be available in order to find all three pairs. Afterwards, the ⟨100⟩ directions $\vec{v_{100}}$ are calculated as the cross product of both pairs vectors $\vec{v_1}$ and $\vec{v_2}$:

$$\vec{v_{100}} = \vec{v_1} \times \vec{v_2} \tag{2}$$

The transformation matrix M can now easily be obtained as:

$$M = \begin{bmatrix} v_{x_{100}} & v_{y_{100}} & v_{z_{100}} \\ v_{x_{010}} & v_{y_{010}} & v_{z_{010}} \\ v_{x_{001}} & v_{y_{001}} & v_{z_{001}} \end{bmatrix} \tag{3}$$

The assignment of the vectors to a certain row is of arbitrary nature, which can cause a negative determinant. It is possible to avoid this issue by calculating the determinant and checking whether it is negative or not. In the case that it results negative, the algorithm inserts $-\vec{v_{100}}$ in the first row instead of $\vec{v_{100}}$. The matrix M is not necessarily a pure rotation matrix because the atoms can assume non perfect lattice positions due to elastic distortions or thermal vibrations. For this reason, we have to estimate the rotation that best fits the affine transformation defined by matrix M. This problem is well known in aeronautics and thus, several solutions have been already provided in the past. For instance, Horn [71] introduced a direct method that estimates an orientation

from a set of corresponding vectors in two coordinate systems for aeronautical purposes. A similar method that requires computing the eigenvalues of a 4×4 matrix was presented by Bar-Itzhack [72]. This method is based on the q-method proposed by Keat [73]. We opted to use this method in the present contribution as operations with quaternions are computationally less expensive. The q-method utilizes a cost function c to be minimized:

$$c = \frac{1}{2} \sum_{i=1}^{k} a_i |\vec{b_i} - D(q)\vec{r_i}|^2 \tag{4}$$

where $\vec{r_i}$ denotes a unit vector in the reference/sample coordinate system and $\vec{b_i}$ the same vector in the body/crystal coordinate system. In turn, q is the sought rotation quaternion, which defines the rotation matrix D whereas a_i is an optional weight to each of the vector pairs. The cost function contains the square lengths of the error vectors, i.e. the minimization is applied with the Euclidean norm. In [73], it was shown that the solution of this problem is reduced to the computation of the eigenvalues of a symmetrical 4×4 matrix, which is defined by the set of vectors $\vec{r_i}$ and $\vec{b_i}$. To find the best-fitting rotation quaternion to the transformation matrix, the method introduced in [72] was utilized. In this contribution, it was shown that by utilizing the three base vectors [100], [010] and [001] of the reference coordinate system, the problem can be formulated for non-orthogonal matrices. As a result, the new matrix M_4 can be computed from the values of the matrix M from Eq. (3) as:

$$M_4 = \frac{1}{3} \begin{bmatrix} r_{11} - r_{22} - r_{33} & r_{21} + r_{12} & r_{31} + r_{13} & r_{23} - r_{32} \\ r_{21} + r_{12} & r_{22} - r_{11} - r_{33} & r_{32} + r_{23} & r_{31} - r_{13} \\ r_{31} + r_{13} & r_{32} + r_{23} & r_{33} - r_{11} - r_{22} & r_{12} - r_{21} \\ r_{23} - r_{32} & r_{31} - r_{13} & r_{12} - r_{21} & r_{11} + r_{22} + r_{33} \end{bmatrix} \tag{5}$$

The quaternion q representing the rotation that best fits M is the eigenvector of the most positive eigenvalue of M_4. The determined quaternion q is then assigned to the current atom during the calculation. In the case that the matrix

M cannot be defined owing to strong lattice distortions, the corresponding atom is marked as non-oriented.

2.2. Grain detection

After the assignation of the orientation to the atoms, the grains are identified in a second step. The identification method uses the orientation information generated in the previous step. The procedure begins from an initial atom as a seed and recursive assignations are applied to nearest-neighbor atoms. For this, the following steps are conducted:

1. Check whether the nearest-neighbor atoms to a seed atom:
   (a) are not yet assigned to another grain-entity.
   (b) own an orientation close to the seed-atom according to a user defined threshold (1° as default). This is referred to as the *local criterion*.
   (c) own an orientation close ($< 3°$ as default) to the mean orientation of the current grain if and only if enough atoms have been aggregated to this grain. This is referred to as the *global criterion*.
2. If these conditions are fulfilled, the neighbor atom is aggregated. The procedure is now repeated from the beginning with the aggregated atoms as seeds.

This procedure is exercised for every atom in the data set. It can occur during an iteration that the number of aggregated atoms of a grain is smaller than a reasonable amount (200 atoms as default). Whenever this happens, the corresponding grain information is removed and all collected atoms during this step are set to be unassigned again.

In Fig. 2, the application of the misorientation criteria is exemplified. The *local criterion* compares the orientation of two atoms in a nearest-neighbor relationship whereas the *global criterion* assures that the orientation of an atom to be aggregated has a similar orientation than that of the current grain. The *global criterion* allows for the detection of grains separated by low angle grain

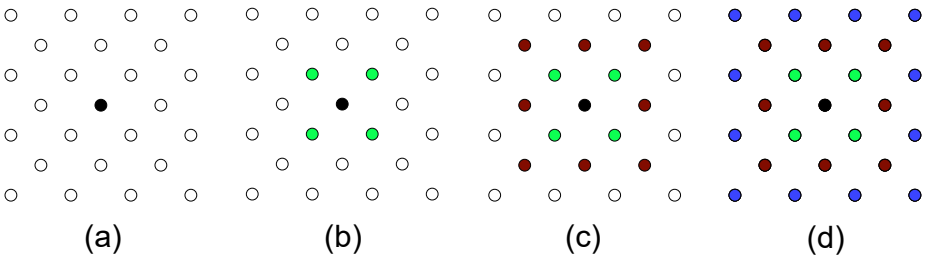

Figure 1: Sequence for the identification of the grains. (a) A seed atom is selected from the dataset; open circles represent atoms with the same orientation as the seed atom. (b) The first neighbors to the seed are identified by comparison of the per-atom orientations and collected into a grain entity. (c-d) In subsequent iterations, the already identified atoms (green in (c), brown in (d)) act as seeds for their next-neighbors. Atoms are continually collected until no equally oriented atoms can be found in an iteration step.

boundaries, which otherwise cannot be detected only by local comparisons due to the gradual change of orientation between grains at positions far away from dislocation centers.

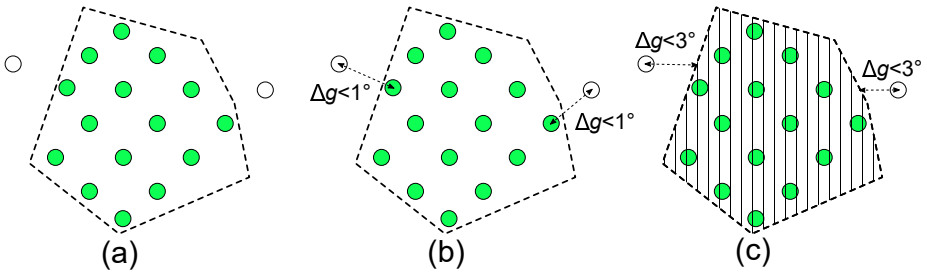

Figure 2: A fully identified grain (a) consists of the atoms (solid circles) enclosed by the dashed line after few iterations. Nearest-neighbors to the already aggregated atoms are tested in subsequent iterations. In order to collect an atom to the current grain entity, the atom must have an orientation difference less than 1° with respect to the seed atom (b) and additionally ensure that the orientation difference with respect to the mean orientation of the grain is less than 3° (c).

2.3. Orphan atom adoption

In some cases owing to strong thermal vibrations or proximity to lattice defects, the determination of the orientation can fail or deliver orientations different than those found in an immediate neighborhood. In both cases, such atoms will not be assigned to a grain entity during the grain identification step. These atoms, deemed in the following as *orphan atoms*, can cause a substantial underestimation of the volume of the grains. To solve this problem, we utilized a method inspired in noise correction methods used in EBSD mapping algorithms [74, 75]. The approach consists of the following steps:

(a) For each orphan atom, the grains to which the nearest neighbors belong are identified and counted.

(b) From the list of grains determined in the previous step, the one with most occurrences is selected.

(c) If the maximum number of occurrences is higher than a user defined value (the default is three), the orphan atom is assigned to the grain selected in step (b).

(d) The procedure is repeated for all remaining orphan atoms.

The minimum number of grain occurrences (three) was introduced in order to suppress random grain assignations. This procedure is schematically shown in Fig. 3. Note that initially (Fig. 3b) only orphan atoms a_A and a_B are adopted because only they had enough nearest neighbors assigned to a common grain. This procedure is applied iteratively so that the number of orphan atoms is reduced to a minimum.

The adoption procedure is expected to introduce an error to the shape of the grain boundaries and triple lines as the assignation of the atoms is not anymore perfectly deterministic. Nevertheless, this error is estimated to be negligible as its possible magnitude is in the range of the lattice parameter whereas the dimension of triple lines and grain boundaries are several times that scale and is comparable to the grain size. For an exact quantification of the error, the

identification of the structural elements of the microstructure is necessary. This feature is not yet implemented in the program.

2.4. Grain-tracking over time

In order to determine the evolution of grain properties over time, it is necessary to track the grains from snapshots generated at different times. To do this, we assume that geometrical and orientation attributes of the grains show little change between subsequent time states. This enables finding correspondence of grains by comparing calculated properties. We utilized two criteria to identify possible corresponding candidates, namely the center-of-mass (COM) and the misorientation between grain candidates. To begin with, the COM of the grains is calculated for the data sets generated at times t and $t + \Delta t$. An arbitrary grain G_1 is selected from the second data set $(t + \Delta t)$. From the first one (t), the grains that fulfill $d \leq d_{max}$, where d is the distance to grain G_1 and d_{max} is a user defined threshold value, are chosen. This list is further refined by rejecting grains with a misorientation larger than a user-defined value ($\Delta g > 5°$ as default). If more than one grain exist that fulfill both criteria, the grain with the shortest distance d is chosen.

The methods described in the previous sections are provided as pseudo-code in the appendix and implemented as a command-line program called GraDe-A (Grain Detection Algorithm). The program was written in the object-oriented C++ programming language. Furthermore, the software uses shared-memory parallelization by means of the OpenMP-API [76], which enables analyzing several input files in parallel. The code has been written accounting for computation time considerations. Thereby, the utilization of computationally slow operations such as square root or cosine calculations has been avoided. Additionally, the computation domain has been split into cells in order to accelerate nearest-neighbor-search algorithms. All orientation data is internally stored as unit quaternions with memory consumption for only four floating-point numbers. Therefore, all misorientation calculations are implemented as simple quaternion operations, which are superior to rotation matrix operations with regard to

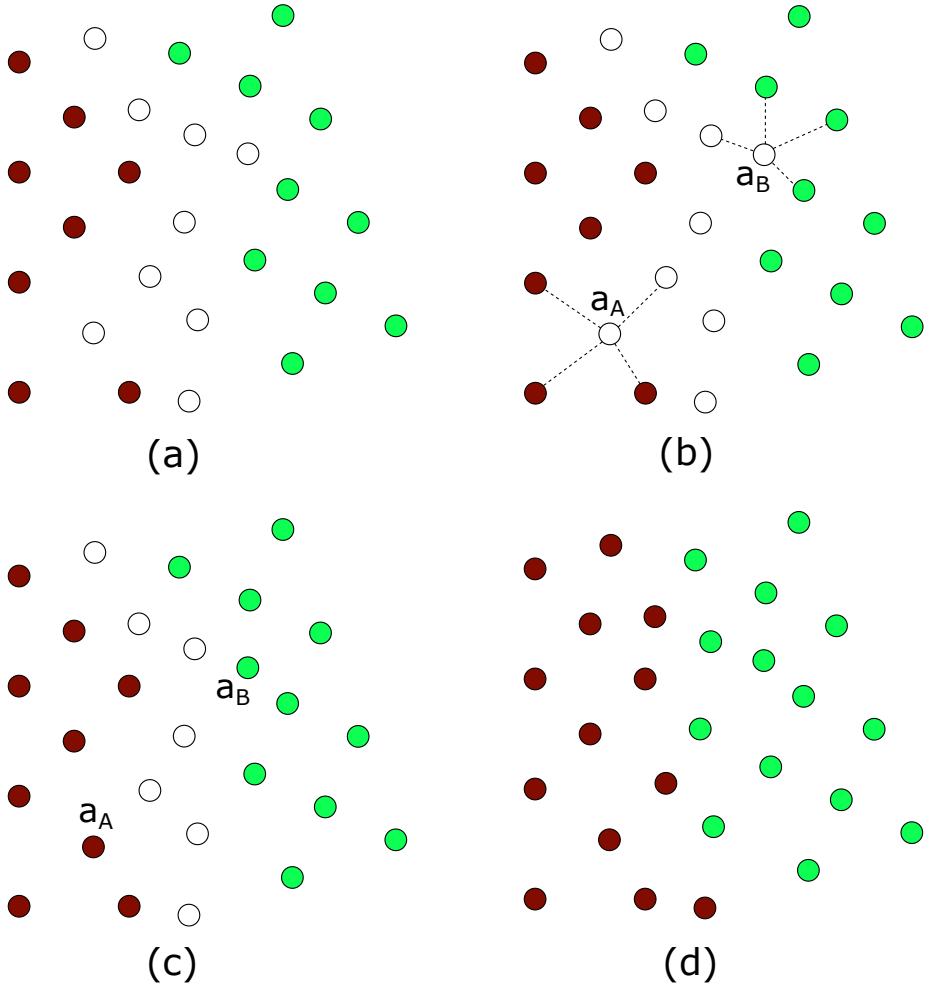

Figure 3: Adoption of orphan atoms. The orphaned state is represented by open circles whereas differently colored circles signify atoms aggregated to different grains. (a) Initially, many atoms close to grain boundaries are not assigned to a specific grain. These atoms are adopted recursively depending on the frequency occurrences to neighboring grains (b). For example, in (c) atom a_A is adopted by the grain on the left whereas atom a_B is adopted by the grain on the right. After a few iterations the number of orphan atoms is reduced to a minimum (d).

computational effort. Unique cubic orientation quaternions (see A6) [77] are used in order to be able to calculate the mean-orientation and the orientation spread [77] for each grain. Additionally, this enables to use a fast disorientation calculation for the grain identification algorithm. The code is also offered as open-source software [70].

2.5. Molecular dynamics simulations of grain growth

Molecular dynamics simulations were employed to test the developed software. For this purpose, nanocrystalline grain growth was simulated. The large-scale atomic/molecular massively parallel simulator (LAMMPS) code [78] was utilized. The atomic interactions were described by the EAM potential for Al developed by Mishin et al. [63]. The algorithms presented in previous sections were used to determine the orientation of grains in an Al polycrystal and reconstruct them in time-resolved molecular dynamics data sets [70]. The simulation block used in these MD simulations was composed of one hundred Voronoi grains with different orientations (Fig. 4) that were defined so that a weak texture was predominant in the microstructure. The orientations were assigned randomly to the grains. The simulation box had a side length of 43.27 nm in all directions and contained 4834137 atoms for an initial average grain size of approximately 11.57 nm. Periodic boundary conditions were used on all the surfaces of the simulation box. Before the MD simulation was performed, the energy of the system was minimized by the conjugate-gradient algorithm. Subsequently, damped dynamics were applied to fully relax the grain boundaries. The isothermal-isobaric (NPT) ensemble was used for the time integration with a time step of 0.2 fs. The simulation was performed at 500 °C. The total simulation time corresponded to 4 ns. In order to warrant the accuracy of the measured properties of the simulated systems, snapshots were regularly saved in intervals of 0.01 ns. The obtained configurations were subsequently quenched computationally in an NPT-ensemble for a time of 0.1 ns to a target temperature of 1 K and additionally relaxed by the conjugate gradient algorithm after setting the kinetic energy to zero. For the identification of the grains, the de-

fault thresholds were consistently used for all of the data analyzed. An amount of 200 atoms was set as a minimum for any grain detection.

The MD-simulations were performed on the Jülich Supercomputing Cluster and the post-processing of the data on the RWTH-Aachen Computer Cluster.

3. Results

3.1. Validation and computational performance

The algorithm was benchmarked on a Bull MPI-S machine possessing Intel Xeon X5675 processors. For these tests, we used 24 files of approximately 240 MB containing ∼4.8 million atoms. The utilized parallelization scheme allowed reducing the computation time from 1.02 hours for two threads to only 12 minutes for 12 threads (Table 1). Irregular scaling with the number of threads was observed. This behavior was caused by an asymmetrical distribution of tasks per thread seen in situations where the number of tasks is not a multiple of the number of threads e.g. 10 threads. This problem is less significant with an increasing number of tasks. For instance, in the present contribution a total of 400 files for a total data volume of 140 GB were evaluated in only approximately 4 hours.

To estimate the accuracy of the algorithm, the determined orientations were compared to the ones used as input. It is stressed that the algorithm does not require initial orientations as input. The figures plotted in Fig. 4 illustrate clearly that the algorithm is capable to identify correctly the orientations of the grains. Fig. 4a and Fig. 4b correspond respectively to the seeded orientations and the orientations calculated from the MD data set. Fig. 4c shows the microstructure colored after the identification number of the grains, which is a number determined by the sorted volume of the grains. This is the reason, why large grains appear blue and small red. The identification number can change from one snapshot/time-step to another due simply to the growth and shrinkage of the grains. However, as explained in the previous section the algorithm is capable of tracking correctly the grains as the COM and orientation are the criteria

Table 1: Comparison of the total computation time t_{comp} necessary for processing 24 output-files by the Grade-A tool. A different number of threads (#Th) were used for benchmarking in a linux-environment with 12 CPU-cores. Each file contained about 4.8 million atoms and had a size of approximately 240 MB. The relative overhead was calculated using the computation with two threads as reference.

#Th	$t_{comp}(h)$	$t_{comp}\times$#Th (h)	Overhead (%)
2	1.02	2.03	0.00
4	0.53	2.12	3.78
6	0.37	2.23	9.469
8	0.29	2.28	12.17
10	0.28	2.77	36.10
12	0.20	2.43	19.29

utilized for the tracking, independently of the identification number assigned at a time step.

Clearly, the advantage of the grain reconstruction is that it makes possible the tracking of grain properties such as volume, center of mass, average orientation, orientation spread and orientation change. Additionally, the algorithm permits the identification of sudden events that influence decisively the development of the microstructure. For instance, Fig. 5a illustrates the global kinetics obtained by detecting the remaining grains at each snapshot of the simulation. It is noted that since grains are individually identified, other algorithms for grain size measurements, such as fitting ellipsoids to the grains [79], can be easily implemented.

3.2. Grain growth kinetics and rotation

From initial 100 grains in the microstructure, the number of grains decreased to only 40 after 4 ns. Figure 5a reveals the average of the grain volume with time whereas Fig. 5b shows the individual kinetics of the detected grains. Note

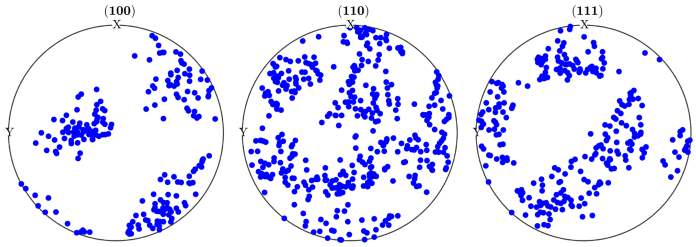

(a)

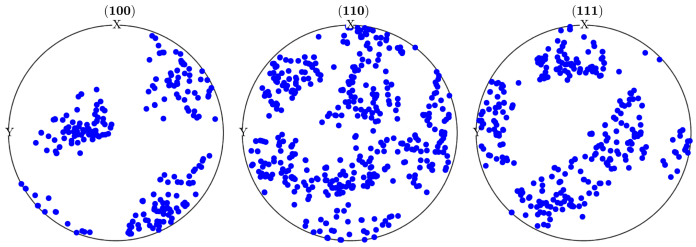

(b)

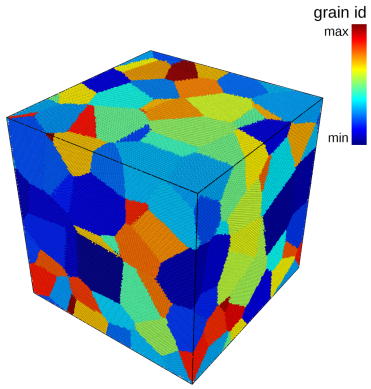

(c)

Figure 4: (a) The input orientation are shown in the pole figures and (b) compared to the determined orientations by the GraDe-A tool. An excellent agreement can be observed. The reconstruction of the grains is seen in (c), where the grains are colored according to an integer number that serves as an id for the grains. This number was assigned so that the smallest number corresponds to grains with the largest volume and vice versa.

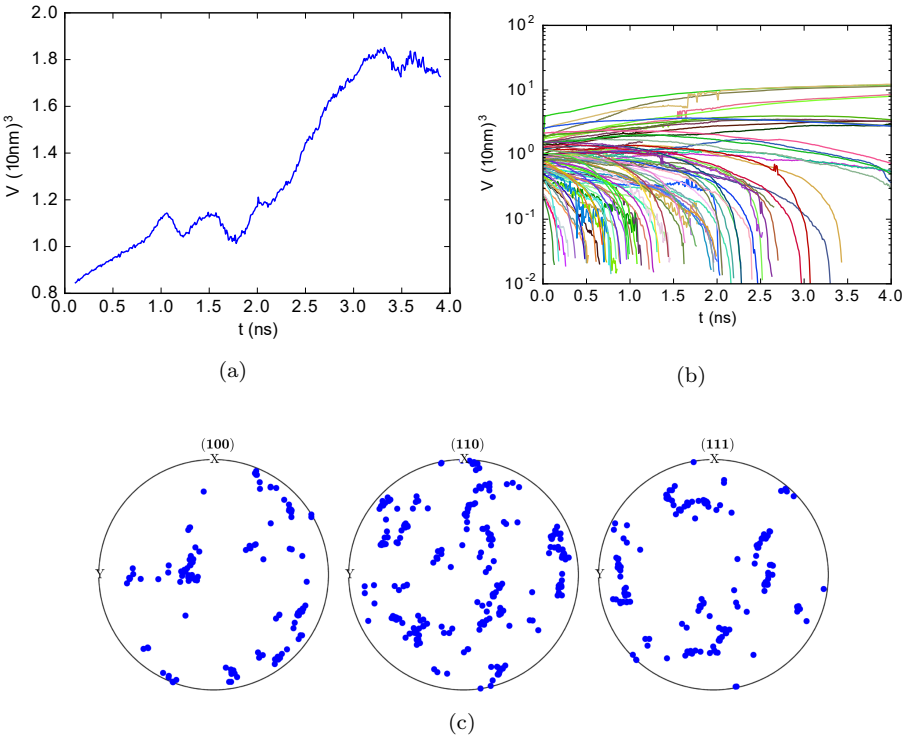

Figure 5: (a) Global kinetics, (b) individual kinetics and final texture (c) after 4 ns of computational annealing at 500 °C. Fluctuations observed in the development of the kinetics are caused by the reconstruction algorithm and thermal fluctuations as grains with approximately 200 atoms can suddenly gain or lose atoms and thus be discriminated as either valid or invalid grains. It is noted that the moving average is shown in (a); as the amount of grains is small, the fluctuations appear more pronounced.

that the ordinate is in logarithm scale so that the collapse of the grains is better visualized. For comparison, the orientations of the remaining grains after the finalization of the simulation are plotted in the pole figures shown in Fig. 5c; a slight sharpening of the initially used weak texture is evident as expected for the texture evolution after grain growth [38]. Remarkably, the evolution of the grains seems to agree qualitatively very well with simulations performed

by mesoscopic simulation models [34], where the kinetics of individual grains were also compared. In addition, the individual volume evolution of the grains is in accordance to theoretical expectations [80, 81, 82, 83, 84, 85, 86]. However, differences become evident, when the evolution in time of the grain volume is analyzed in detail as discussed below. Since the algorithm is capable of determining a per-atom orientation and identify the grains, it is also possible to determine any change in orientation that might be induced during grain growth. This is a topic of interest because Cahn and Taylor [87] predicted that rotation of grains can be caused by the motion of grain boundaries. Several simulation studies [64, 65, 88, 66, 26] and some experimental ones [89, 90, 91] have confirmed this effect for stressed nanocrystalline polycrystals. However, other experimental studies [91] have not observed this concomitant grain migration and rotation in systems closer to the simulated ones, where rotation is thought to be more prominent. In fact, in previous simulation studies [66, 92], we showed that rotation is strongly dependent on the character of the grain boundary. Furthermore, most of the computational studies have been performed in bi- or tricrystals [88] and with CSL grain boundaries as a necessity to fulfill periodicity on all surfaces of the simulation setups. However, grain boundaries in real microstructures tend to be of a mixed and general character and can deviate substantially from CSL or Σ grain boundaries. For this reason, it is unclear whether grain rotation will be observed as a generalized mechanisms of microstructure evolution. To investigate if grain rotation is observed in nanocrystalline polycrystals subjected to grain growth, we tracked the orientation change of the grains. In Fig. 6a the average absolute change of grain orientation as a function of time is shown. The maximum orientation change was less than 3.5°; this evinced only a marginal orientation change that is not in accordance with Cahn and Taylor theoretical expectations [87, 66, 92, 65]. The reason for this may be related to the structure of the grain boundaries as discussed in [66] but a more detailed investigation of the mechanisms of grain boundary migration is necessary to affirm this. As for the kinetics, the change of orientation can also be resolved for individual grains. This is illustrated in Fig. 6b, where the rotation of all the grains in

the simulations is plotted as a function of time. Interestingly, rotation is most prominent for grains that are close to collapse as evinced by those grains, whose orientation change increases in a very short time. An important difference with respect to the simulations by Haslam et al. [93] is that grain coalescence was not substantially observed. The reason for this is that Haslam simulated quasi-2D grain growth. In addition, all the grain boundaries in their microstructure were tilt boundaries, in which case, grain rotation is inevitable as discussed in [66]. In the present simulations most of the grain boundaries possess mixed grain boundaries as a result of the dimensionality of the microstructure, which results in a microstructure closer to real polycrystals. The effect of a mixed component of the grain boundary on grain rotation has been studied previously [29, 66]. These studies indicated that mixed grain boundaries with common $< 100 >$ rotation axis do not rotate by the capillary motion of the boundary. The fact that in our simulations no substantial rotation was observed seems to support this previous conclusion.

Finally and to give an impression of the practicality of the algorithm, individual grain kinetics and orientation change for an arbitrary grain are shown in Fig. 6c and Fig. 6d. This representation makes possible identifying significant but rare events that are determinant for microstructure evolution [93, 48, 94, 49]. In the case of this grain, the kinetics showed an initial fast growth until it reached a constant volume from approximately 2 to 2.5 ns. Afterward, the grain shrank until the simulation finished. The morphology of this grain can be seen in Fig. 7. This grain was able to survive the whole simulation and grew successfully for most of its life reaching a maximum grain size after 2.66 ns (Fig. 7c). This growth is also substantiated by the number of faces that the grain gained. For instance, after 1.33 ns (Fig. 7b) the grain had significantly more faces than originally (Fig. 7a) and evidently a concave shape that signifies positive growth rates. At the last simulated time (Fig. 7d), the grain had already started shrinking showing a smaller size than at a previous time (Fig. 7c) and also a convex shape. Note that the shape is not irregular and approximates excellently grains observed in polycrystals by serial-sectioning or tomography [95, 96, 97]. This

is also an indication that the software can identify and reconstruct the grains adequately.

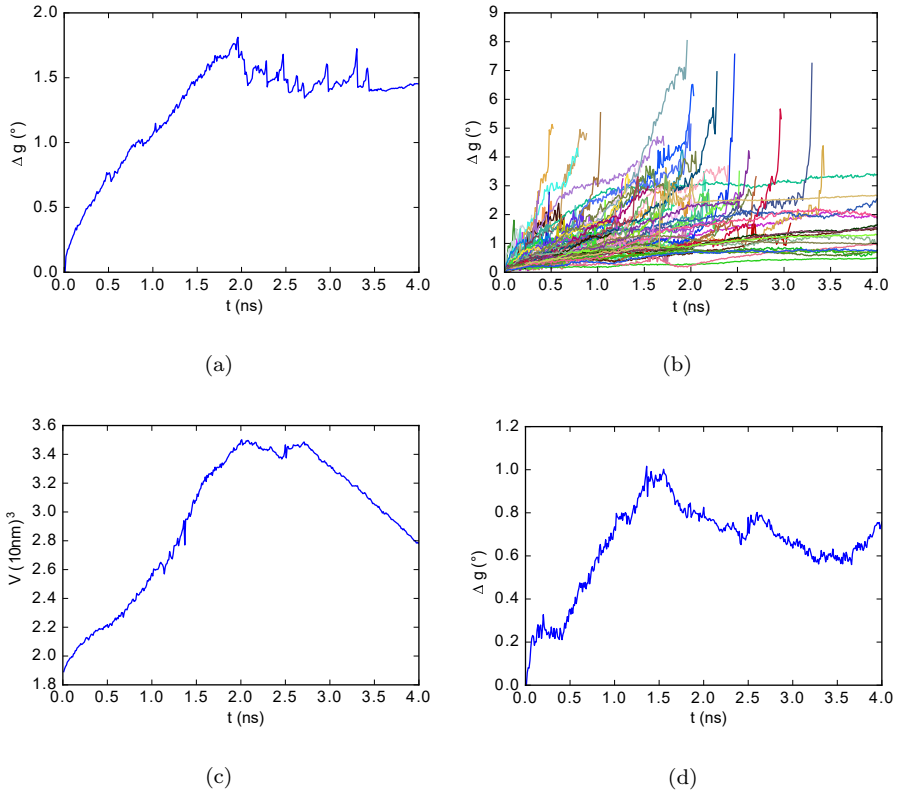

Figure 6: (a) Average grain rotation and (b) individual rotation of the grains. Grain rotation seems to increase with decreasing grain size of the grains. However, the average orientation change of the grains remains below 3.5°. Significant events for microstructure evolution can also be identified since properties such as kinetics (c) and orientation change (d) of the grains are individually resolved. In (c) and (d), the properties plotted correspond to the grain shown in Fig. 7

.

The stagnation of the growth of this grain is also evident at about $t \approx 2.0$ ns. It is impossible to separate the topology of the grain to the growth rate of the grain [98]. However, it is also evident from the global kinetics (Fig. 5)

that grain growth did not occur ideally, which indicated a deviation from the theoretical expectations. Owing to the low number of grains in the microstructure, the observed tendencies and in particular the deviations may be caused by an insufficient sample size. However, in the simulations it was always possible to associate the retardation events to specific occurrences of grain boundary migration. For instance, an inspection of the microstructure during grain growth revealed that also inherent features of the grain boundaries such as grain boundary dislocations can affect grain boundary motion and thus, grain growth. From the sequence shown in Fig. 8, it was possible to associate the stagnation of grain growth to the emission of dislocation from one of the grain boundaries in addition to the change of topology that occurred at a later time (Fig. 8c and Fig. 8d). For a discrimination of topological effects, the determination of the topology of the grains is necessary. This task is not trivial as not only the neighborhood of the grains but also their metrics must be determined [98, 99]. More intriguing is the effect of the initial microstructure, which was generated from a Voronoi tessellation. It is well known that the grain size distribution of Voronoi mosaics deviate strongly from the equilibrium distribution of normal or ideal grain growth. It might, of course, be argued that under experimental and the used simulation conditions no ideal grain growth can be expected. However, a transient from the initial to the equilibrium distribution can still be anticipated. Previous investigations [11, 100] by mesoscopic simulations have substantiated that an initial non-equilibrium grain size distribution can considerably affect the evolution of grain growth especially in nanocrystalline materials. For instance, the increase of faces during the growth of the grain in Fig. 7 is a feature that was already observed in simulations of early regimes of grain growth [100]. Nevertheless, from only one case of study, it is difficult to determine the extent of the effect of the initial microstructure. To study this and also the possible effects caused by the dimensionality of the sample, MD simulations of the same microstructure but with different initial grain size would be necessary. These simulations are at the moment being performed and we expect to report on them soon.

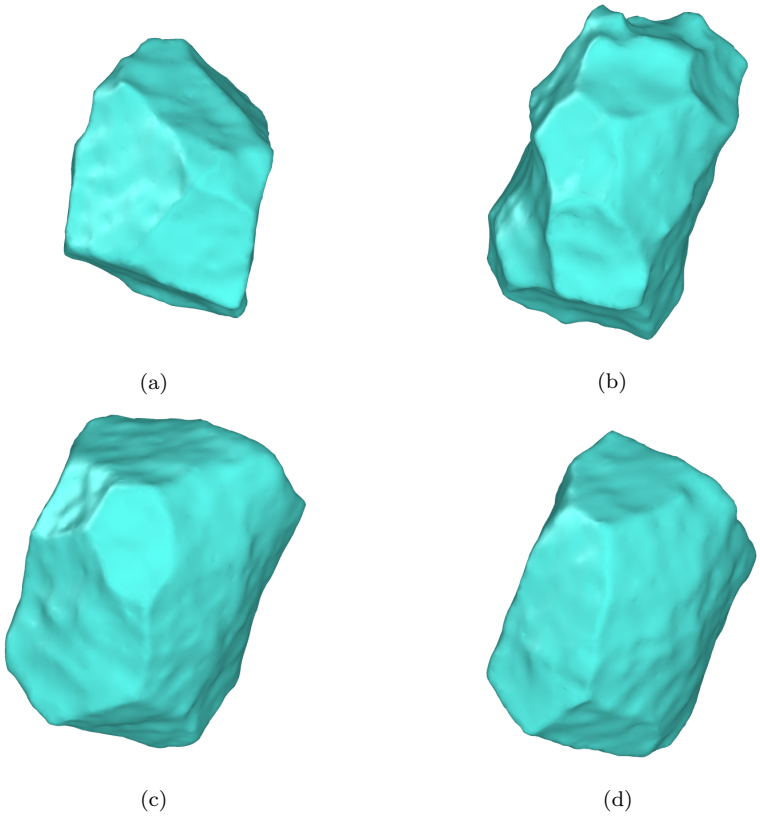

Figure 7: Development of an arbitrary grain as reconstructed by the GraDe-A tool. The surface was calculated by means of the visualization software OVITO [101]. This grain initially grew (b) until it reached a maximum number of faces after 1.33 ns and a maximum size (c) after 2.66 ns. Afterward, the grain shrank (d) until the simulation finalized after 4 ns.

The purpose of this manuscript was to study grain growth by molecular dynamics simulations in a nanocrystalline polycrystal. For this purpose, we introduced the computational tool GraDe-A for the determination, reconstruction and tracking of grains in FCC polycrystals from MD data sets. This tool was utilized to evaluate the change of properties of the grains. We expect this tool to become a valuable tool for the interpretation of data from MD simulations and

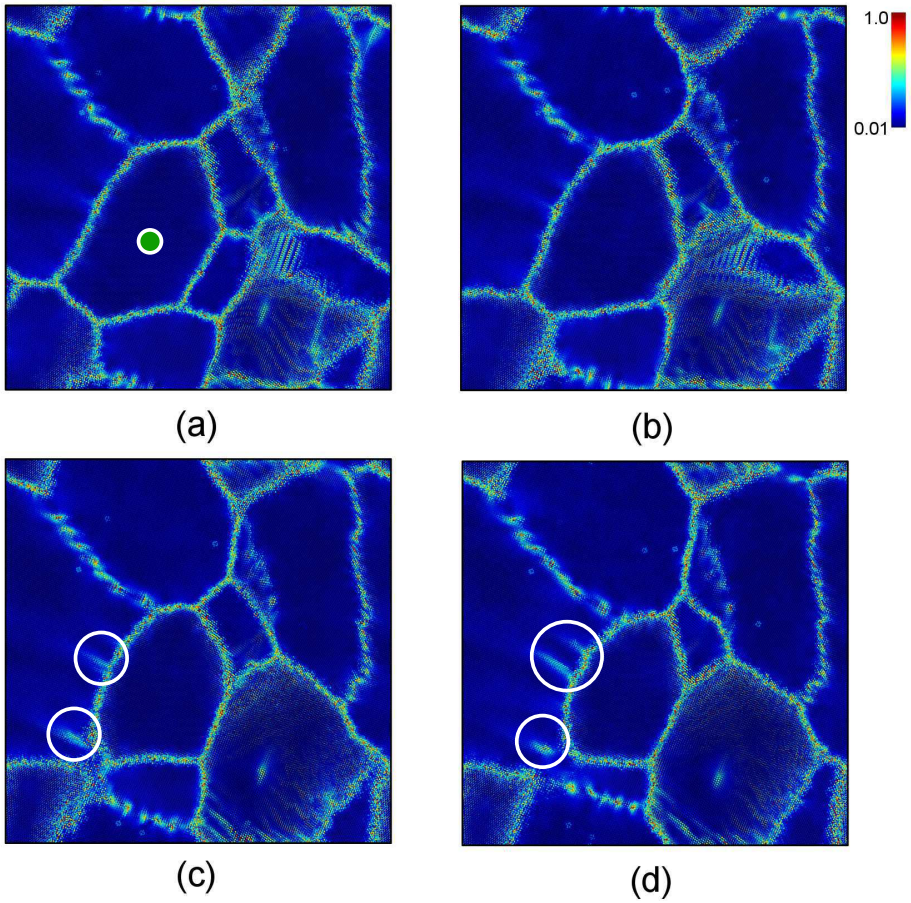

Figure 8: (a) The grain with the solid circle in its interior corresponds to the same grain in Fig. 7 after $t = 2.23\ ns$. At this time, the growth rate is constant. Little change volume is observed even after $t = 2.65\ ns$ (b). One of the causes is apparently the dragging effect of grain boundary dislocations (white circles) (c) that must be emitted from the grain boundary before boundary migration can proceed at faster rates (d). In this figure, the grains were colored according to the von Mises stress in the grains. It is evident that no substantial changes of stress inside the grains is observed.

the community is invited to contribute to the project [70]. In addition, recently also a tool capable of discerning orientation from MD datasets was developed

[102], which in conjunction with the tool introduced here would allow analyzing grains in polycrystals with different crystal structures.

4. Summary

A computational tool, which is capable of identifying grain entities by the calculation of per-atom orientation quaternions, was developed. It was demonstrated that the tool is powerful enough to allow for grain-resolved 3D-visualizations of the grains and that it provides useful grain-quantities, such as mean-orientation, volume and rotation angles. A Voronoi-tesselated microstructure with a weak texture was synthesized and used to simulate grain growth at 500 °C by molecular dynamics; snapshots from these simulations were used to benchmark the computational tool. The developed algorithm was used to determine global and per-grain kinetics and mean rotation of the grains.

The results of the simulations substantiate non-linear grain growth kinetics. This behavior was attributed to the dragging of grain boundary dislocations on boundary migration that resulted in decreased kinetics. Additionally, grain rotation was found not to occur significantly and thus grain coalescence occurred only rarely during grain growth in contradiction to the observations by Haslam et al. [94].

Regarding the computational tool GraDe-A, there are various improvements and extensions that are currently under development:

- Add support for other lattice-structures
- Identifying and highlighting other network-entities such as faces, edges and junctions
- Calculate grain-properties such as triple line length, turning angle and mean width
- Obtaining topological and connectivity-information for each grain
- Calculating the 5 parameter space of grain boundaries

- Determination of Bernal structures of grain boundaries
- Automatically identify grain-coalescence events

These enhancements would be helpful for the analysis of nanocrystalline grain growth and grain rotation since most of the processes observed are difficult to discuss without knowing exact information on the involved defects and geometries.

Acknowledgements

The authors express their gratitude to the Deutsche Forschungsgemeinschaft (DFG) for financial support (Grants GO 335/44-1) and gratefully acknowledge the computing time granted (JHPC24) by the John von Neumann Institute for Computing (NIC) provided on the supercomputer JURECA at Jülich Supercomputing Centre (JSC). P. W. Hoffrogge thankfully acknowledges the computing time granted by the RWTH-Aachen University (RWTH0060) for the execution of his master-thesis project.

References

References

[1] H. Paul, C. E. Krill, Anomalously linear grain growth in nanocrystalline fe, Scripta Materialia 65 (2011) 5–8.

[2] M. Ames, J. Markmann, R. Karos, A. Michels, A. Tschpe, R. Birringer, Unraveling the nature of room temperature grain growth in nanocrystalline materials, Acta Materialia 56 (2008) 4255–4266. Acta Mater.

[3] C. E. Krill, L. Helfen, D. Michels, H. Natter, A. Fitch, O. Masson, R. Birringer, Size-dependent grain-growth kinetics observed in nanocrystalline fe, Phys. Rev. Lett. 86 (2001) 842–845.

[4] M. Saber, C. C. Koch, R. O. Scattergood, Thermodynamic grain size stabilization models: An overview, Materials Research Letters 3 (2015) 65–75.

[5] R. A. Andrievski, Review of thermal stability of nanomaterials, J Mater Sci 49 (2013) 1449–1460.

[6] S. Simoes, R. Calinas, M. T. Vieira, M. F. Vieira, P. J. Ferreira, In situ tem study of grain growth in nanocrystalline copper thin films, Nanotechnology 21 (2010) 145701. Nanotechnology.

[7] L. A. Barrales Mora, G. Gottstein, L. S. Shvindlerman, Understanding grain boundary junctions: Effect of the grain size on microstructure evolution, Materials Science Forum 715 (2012) 186–190.

[8] L. A. Barrales Mora, V. Mohles, L. S. Shvindlerman, G. Gottstein, Effect of a finite quadruple junction mobility on grain microstructure evolution: Theory and simulation, Acta Materialia 56 (2008) 1151–1164.

[9] L. A. Barrales Mora, L. S. Shvindlerman, V. Mohles, G. Gottstein, The effect of grain boundary junctions on grain microstructure evolution, Materials Science Forum 558-59 (2007) 1051–1056.

[10] L. A. Barrales-Mora, G. Gottstein, L. S. Shvindlerman, Effect of the energy of triple-lines on 3d grain growth, Materials Science Forum 753 (2013) 373–376. Mater Sci Forum.

[11] L. A. Barrales-Mora, G. Gottstein, L. S. Shvindlerman, Effect of a finite boundary junction mobility on the growth rate of grains in two-dimensional polycrystals, Acta Materialia 60 (2012) 546–555. Acta Mater.

[12] L. A. Barrales-Mora, G. Gottstein, L. S. Shvindlerman, Effect of finite boundary junction mobility on the growth rate of grains in 3d polycrystals, Philosophical Magazine 92 (2012) 1046–1057. Philos Mag.

[13] U. Czubayko, V. G. Sursaeva, G. Gottstein, L. S. Shvindlerman, Influence of triple junctions on grain boundary motion, Acta Materialia 46 (1998) 5863–5871.

[14] G. Gottstein, Y. Ma, L. Shvindlerman, Triple junction motion and grain microstructure evolution, Acta Materialia 53 (2005) 1535–1544.

[15] G. Gottstein, L. S. Shvindlerman, Triple junction drag and grain growth in 2d polycrystals, Acta Materialia 50 (2002) 703–713.

[16] G. Gottstein, L. S. Shvindlerman, B. Zhao, Thermodynamics and kinetics of grain boundary triple junctions in metals: Recent developments, Scripta Materialia 62 (2010) 914–917.

[17] B. Zhao, G. Gottstein, L. S. Shvindlerman, Triple junction effects in solids, Acta Materialia 59 (2011) 3510–3518. Acta Mater.

[18] B. Zhao, J. C. Verhasselt, L. S. Shvindlerman, G. Gottstein, Measurement of grain boundary triple line energy in copper, Acta Materialia 58 (2010) 5646–5653.

[19] G. Gottstein, L. Shvindlerman, Grain boundary junction engineering, Scripta Materialia 54 (2006) 1065–1070.

[20] G. Gottstein, A. King, L. Shvindlerman, The effect of triple-junction drag on grain growth, Acta Materialia 48 (2000) 397–403.

[21] V. Novikov, On the influence of triple junctions on grain growth kinetics and microstructure evolution in 2d polycrystals, Scripta Materialia 52 (2005) 857–861.

[22] V. Novikov, On grain growth in the presence of mobile particles, Acta Materialia 58 (2010) 3326–3331.

[23] V. Y. Novikov, Grain growth jointly affected by immobile and mobile particles, Materials Letters 178 (2016) 276–279.

[24] L. Klinger, E. Rabkin, L. S. Shvindlerman, G. Gottstein, Grain growth in porous two-dimensional nanocrystalline materials, J Mater Sci 43 (2008) 5068–5075.

[25] N. Bernstein, The influence of geometry on grain boundary motion and rotation, Acta Materialia 56 (2008) 1106–1113.

[26] M. Upmanyu, D. J. Srolovitz, A. E. Lobkovsky, J. A. Warren, W. C. Carter, Simultaneous grain boundary migration and grain rotation, Acta Materialia 54 (2006) 1707–1719.

[27] E. A. Holm, S. M. Foiles, How grain growth stops: a mechanism for grain-growth stagnation in pure materials, Science 328 (2010) 1138–41.

[28] B. B. Straumal, V. G. Sursaeva, B. Baretzky, Grain boundary ridges and triple lines, Scripta Materialia 62 (2010) 924–927.

[29] L. A. Barrales Mora, D. A. Molodov, Capillarity-driven shrinkage of grains with tilt and mixed boundaries studied by molecular dynamics, Acta Materialia 120 (2016) 179–188.

[30] J. R. Trelewicz, C. A. Schuh, Grain boundary segregation and thermodynamically stable binary nanocrystalline alloys, Phys. Rev. B 79 (2009).

[31] T. Chookajorn, H. A. Murdoch, C. A. Schuh, Design of stable nanocrystalline alloys, Science 337 (2012) 951–954.

[32] H. A. Murdoch, C. A. Schuh, Stability of binary nanocrystalline alloys against grain growth and phase separation, Acta Materialia 61 (2013) 2121–2132.

[33] M. Saber, H. Kotan, C. C. Koch, R. O. Scattergood, Thermodynamic stabilization of nanocrystalline binary alloys, J. Appl. Phys. 113 (2013) 063515.

[34] D. Zöllner, P. Streitenberger, I. Fielden, The kinetics of individual grains in polycrystalline materials, Practical Metallography 49 (2012) 428–445.

[35] R. Darvishi Kamachali, I. Steinbach, 3-d phase-field simulation of grain growth: Topological analysis versus mean-field approximations, Acta Materialia 60 (2012) 2719–2728.

[36] R. D. Kamachali, J. Hua, I. Steinbach, A. Hartmaier, Multiscale simulations on the grain growth process in nanostructured materials, International Journal of Materials Research 101 (2010) 1332–1338.

[37] L. A. Barrales Mora, 2d vertex modeling for the simulation of grain growth and related phenomena, Mathematics and Computers in Simulation 80 (2010) 1411–1427. Math Comput Simulat.

[38] L. Barrales-Mora, 2D and 3D Grain Growth Modeling and Simulation, Cuvillier, Göttingen, 2008. URL: `http://books.google.de/books?id=E3Q0YNZod0wC`.

[39] P. E. Goins, E. A. Holm, The material point Monte Carlo model: A discrete, off-lattice method for microstructural evolution simulations, Computational Materials Science 124 (2016) 411–419.

[40] M. P. Anderson, D. J. Srolovitz, G. S. Grest, P. S. Sahni, Computer simulation of grain growthi. kinetics, Acta Metallurgica 32 (1984) 783–791.

[41] A. D. Rollett, D. J. Srolovitz, M. P. Anderson, Simulation and theory of abnormal grain growthanisotropic grain boundary energies and mobilities, Acta Metallurgica 37 (1989) 1227–1240.

[42] D. Farkas, A. Frøseth, H. Van Swygenhoven, Grain boundary migration during room temperature deformation of nanocrystalline ni, Scripta Materialia 55 (2006) 695–698.

[43] H. V. Swygenhoven, D. Farkas, A. Caro, Grain-boundary structures in polycrystalline metals at the nanoscale, Phys. Rev. B 62 (2000) 831–838.

[44] D. Farkas, S. Mohanty, J. Monk, Strain-driven grain boundary motion in nanocrystalline materials, Materials Science and Engineering: A 493 (2008) 33–40.

[45] J. Monk, D. Farkas, Strain-induced grain growth and rotation in nickel nanowires, Phys. Rev. B 75 (2007).

[46] D. Farkas, S. Mohanty, J. Monk, Linear grain growth kinetics and rotation in nanocrystalline ni, Phys. Rev. Lett. 98 (2007).

[47] D. Farkas, E. Bringa, A. Caro, Annealing twins in nanocrystalline fcc metals: A molecular dynamics simulation, Phys. Rev. B 75 (2007).

[48] A. J. Haslam, D. Moldovan, V. Yamakov, D. Wolf, S. R. Phillpot, H. Gleiter, Stress-enhanced grain growth in a nanocrystalline material by molecular-dynamics simulation, Acta Materialia 51 (2003) 2097–2112. 665TW Times Cited:75 Cited References Count:31.

[49] A. J. Haslam, V. Yamakov, D. Moldovan, D. Wolf, S. R. Phillpot, H. Gleiter, Effects of grain growth on grain-boundary diffusion creep by molecular-dynamics simulation, Acta Materialia 52 (2004) 1971–1987. 814VD Times Cited:24 Cited References Count:56.

[50] V. Yamakov, D. Moldovan, K. Rastogi, D. Wolf, Relation between grain growth and grain-boundary diffusion in a pure material by molecular dynamics simulations, Acta Materialia 54 (2006) 4053–4061.

[51] S. L. Thomas, A. H. King, D. J. Srolovitz, When twins collide: Twin junctions in nanocrystalline nickel, Acta Materialia 113 (2016) 301–310.

[52] H. Zhang, M. Mendelev, D. Srolovitz, Mobility of $\sigma 5$ tilt grain boundaries: Inclination dependence, Scripta Materialia 52 (2005) 1193–1198.

[53] H. Zhang, M. I. Mendelev, D. J. Srolovitz, Computer simulation of the elastically driven migration of a flat grain boundary, Acta Materialia 52 (2004) 2569–2576.

[54] H. Zhang, D. J. Srolovitz, Simulation and analysis of the migration mechanism of 5 tilt grain boundaries in an fcc metal, Acta Materialia 54 (2006) 623–633.

[55] J. D. Honeycutt, H. C. Andersen, Molecular dynamics study of melting and freezing of small lennard-jones clusters, The Journal of Physical Chemistry 91 (1987) 4950–4963.

[56] A. Stukowski, Structure identification methods for atomistic simulations of crystalline materials, Modelling and Simulation in Materials Science and Engineering 20 (2012) 045021.

[57] A. Stukowski, K. Albe, Extracting dislocations and non-dislocation crystal defects from atomistic simulation data, Modelling and Simulation in Materials Science and Engineering 18 (2010) 085001.

[58] C. Begau, J. Hua, A. Hartmaier, A novel approach to study dislocation density tensors and lattice rotation patterns in atomistic simulations, Journal of the Mechanics and Physics of Solids 60 (2012) 711–722.

[59] K. G. F. Janssens, D. Olmsted, E. A. Holm, S. M. Foiles, S. J. Plimpton, P. M. Derlet, Computing the mobility of grain boundaries, Nature Materials 5 (2006) 124–127.

[60] H. Zhang, D. J. Srolovitz, J. F. Douglas, J. A. Warren, Atomic motion during the migration of general [001] tilt grain boundaries in ni, Acta Materialia 55 (2007) 4527–4533.

[61] H. Zhang, M. Upmanyu, D. J. Srolovitz, Curvature driven grain boundary migration in aluminum: molecular dynamics simulations, Acta Materialia 53 (2005) 79–86.

[62] Y. Mishin, M. Asta, J. Li, Atomistic modeling of interfaces and their impact on microstructure and properties, Acta Materialia 58 (2010) 1117–1151.

[63] Y. Mishin, D. Farkas, M. J. Mehl, D. A. Papaconstantopoulos, Interatomic potentials for monoatomic metals from experimental data and ab initiocalculations, Physical Review B 59 (1999) 3393–3407.

[64] Z. T. Trautt, A. Adland, A. Karma, Y. Mishin, Coupled motion of asymmetrical tilt grain boundaries: Molecular dynamics and phase field crystal simulations, Acta Materialia 60 (2012) 6528–6546.

[65] Z. T. Trautt, Y. Mishin, Grain boundary migration and grain rotation studied by molecular dynamics, Acta Materialia 60 (2012) 2407–2424.

[66] L. A. Barrales-Mora, J.-E. Brandenburg, D. A. Molodov, Impact of grain boundary character on grain rotation, Acta Materialia 80 (2014) 141–148.

[67] J. F. Panzarino, J. J. Ramos, T. J. Rupert, Quantitative tracking of grain structure evolution in a nanocrystalline metal during cyclic loading, Modelling and Simulation in Materials Science and Engineering 23 (2015) 025005.

[68] J. F. Panzarino, T. J. Rupert, Tracking microstructure of crystalline materials: A post-processing algorithm for atomistic simulations, JOM 66 (2014) 417–428.

[69] GNU general public license, 2016. URL: `http://www.gnu.org/licenses/gpl.html`.

[70] P. W. Hoffrogge, L. A. Barrales-Mora, Grain reconstruction algorithm for md datasets, https://github.com/paulhof/GraDe-A (2016).

[71] B. K. P. Horn, Closed-form solution of absolute orientation using unit quaternions, Journal of the Optical Society of America a-Optics Image Science and Vision 4 (1987) 629–642. G6126 Times Cited:1602 Cited References Count:15.

[72] I. Y. Bar-Itzhack, New method for extracting the quaternion from a rotation matrix, Journal of Guidance, Control, and Dynamics 23 (2000) 1085–1087.

[73] J. Keat, Analysis of least-squares attitude determination routine DOAOP, Report, Technical Report CSC/TM-77/6034, Comp. Sc. Corp, 1977.

[74] F. J. Humphreys, Grain and subgrain characterisation by electron backscatter diffraction, Journal of Materials Science 36 (2001) 3833–3854.

[75] F. J. Humphreys, Characterisation of fine-scale microstructures by electron backscatter diffraction (ebsd), Scripta Materialia 51 (2004) 771–776.

[76] L. Dagum, R. Menon, Openmp: an industry standard api for shared-memory programming, Computational Science & Engineering, IEEE 5 (1998) 46–55.

[77] J.-H. Cho, A. D. Rollett, K. H. Oh, Determination of a mean orientation in electron backscatter diffraction measurements, Metallurgical and Materials Transactions A 36 (2005) 3427–3438.

[78] S. Plimpton, Fast parallel algorithms for short-range molecular dynamics, Journal of Computational Physics 117 (1995) 1–19.

[79] M. A. Groeber, M. A. Jackson, Dream.3d: A digital representation environment for the analysis of microstructure in 3d, Integrating Materials and Manufacturing Innovation 3 (2014) 5.

[80] M. Glicksman, P. Rios, D. Lewis, Regular n-hedra: A topological approach for analyzing three-dimensional textured polycrystals, Acta Materialia 55 (2007) 4167–4180.

[81] M. E. Glicksman, Analysis of 3-d network structures, Philosophical Magazine 85 (2005) 3–31.

[82] M. E. Glicksman, P. R. Rios, Microstructural characteristics of 3-d networks, Zeitschrift Fur Metallkunde 96 (2005) 1099–1105. Z Metallkd.

[83] M. E. Glicksman, P. R. Rios, Minimal network partitions using average -hedra, Philosophical Magazine 87 (2007) 189–208.

[84] M. E. Glicksman, P. R. Rios, D. J. Lewis, Mean width and caliper characteristics of network polyhedra, Philosophical Magazine 89 (2009) 389–403.

[85] P. R. Rios, M. E. Glicksman, Self-similar evolution of network structures, Acta Materialia 54 (2006) 1041–1051.

[86] P. R. Rios, M. E. Glicksman, Modeling polycrystals with regular polyhedra, Materials Research 9 (2006) 231–236.

[87] J. W. Cahn, J. E. Taylor, A unified approach to motion of grain boundaries, relative tangential translation along grain boundaries, and grain rotation, Acta Materialia 52 (2004) 4887–4898.

[88] Z. T. Trautt, Y. Mishin, Capillary-driven grain boundary motion and grain rotation in a tricrystal: A molecular dynamics study, Acta Materialia 65 (2014) 19–31.

[89] K. E. Harris, V. V. Singh, A. H. King, Grain rotation in thin films of gold, Acta Materialia 46 (1998) 2623–2633.

[90] M. Legros, D. S. Gianola, K. J. Hemker, In situ tem observations of fast grain-boundary motion in stressed nanocrystalline aluminum films, Acta Materialia 56 (2008) 3380–3393.

[91] F. Mompiou, M. Legros, T. Radetic, U. Dahmen, D. S. Gianola, K. J. Hemker, In situ tem observation of grain annihilation in tricrystalline aluminum films, Acta Materialia 60 (2012) 2209–2218.

[92] J. E. Brandenburg, L. A. Barrales-Mora, D. A. Molodov, On migration and faceting of low-angle grain boundaries: Experimental and computational study, Acta Materialia 77 (2014) 294–309.

[93] A. J. Haslam, D. Moldovan, S. R. Phillpot, D. Wolf, H. Gleiter, Combined atomistic and mesoscale simulation of grain growth in nanocrystalline thin films, Computational Materials Science 23 (2002) 15–32. 556VW Times Cited:35 Cited References Count:74.

[94] A. J. Haslam, S. R. Phillpot, H. Wolf, D. Moldovan, H. Gleiter, Mechanisms of grain growth in nanocrystalline fcc metals by molecular-dynamics simulation, Materials Science and Engineering a-Structural Materials Properties Microstructure and Processing 318 (2001) 293–312. 510EX Times Cited:89 Cited References Count:73.

[95] F. N. Rhines, Microstructology: Behavior and microstructure of materials(mikrostruktologie: Gefuge und werkstoffverhalten), Dr. Riederer Verlag GmbH, 1986 (1986) 93.

[96] I. M. McKenna, S. O. Poulsen, E. M. Lauridsen, W. Ludwig, P. W. Voorhees, Grain growth in four dimensions: A comparison between simulation and experiment, Acta Materialia 78 (2014) 125–134.

[97] G. Mbus, B. J. Inkson, Nanoscale tomography in materials science, Materials Today 10 (2007) 18–25.

[98] R. D. MacPherson, D. J. Srolovitz, The von neumann relation generalized to coarsening of three-dimensional microstructures, Nature 446 (2007) 1053–1055.

[99] K. Chang, C. E. Krill Iii, Q. Du, L.-Q. Chen, Evaluating microstructural parameters of three-dimensional grains generated by phase-field simulation or other voxel-based techniques, Modelling and Simulation in Materials Science and Engineering 20 (2012) 075009.

[100] D. Zöllner, P. Streitenberger, P. Rios, Shedding some light on the early grain growth regime: About the effect of the initial microstructure on normal grain growth, Computational Materials Science 113 (2016) 11–20.

[101] A. Stukowski, Visualization and analysis of atomistic simulation data with ovitothe open visualization tool, Modelling and Simulation in Materials Science and Engineering 18 (2010) 015012.

[102] L. Peter Mahler, S. Sren, S. Jakob, Robust structural identification via polyhedral template matching, Modelling and Simulation in Materials Science and Engineering 24 (2016) 055007.

Appendix A. Appendix

Appendix A.1. Per-atom orientation calculation

An orientation is calculated by algorithm A1 for every atom by taking into account the positions of the nearest neighbors. During the calculation a reduced neighbor vector list V_R is calculated for every atom by algorithm A2. This procedure eliminates double occurrences of anti-parallel neighbor unit-vectors by calculating the mean direction $1/2(v_i - v_j)$ of near antipodal pairs. If a sufficient amount of directions remains, the orientation calculator utilizes them to formulate a transformation matrix M, as described in section 2.1. In order to obtain the largest eigenvalue as the resulting quaternion q we use the external open-source linear-algebra solver Armadillo[A1].

[A1] http://arma.sourceforge.net

Algorithm A1: Algorithm calculating the orientation of an atom in a fcc-lattice structured material by taking into account the near neighborhood.

Input: *The antipodal threshold angle $\Delta\alpha$ and the perpendicular threshold angle $\Delta\beta$ in the current work chosen to be 5° and 11.5°, respectively.*

foreach *atom a* **do**
  Identify all n_{NN} nearest neighbor atoms A_{NN}
  Calculate the relative positions V_{NN} of A_{NN} to a
  `// The fcc-lattice has twelve neighbors, too much neighbors may cause problems.`
  if $n_{NN} > 12$ **then**
    return not oriented
  end
  Calculate the unit vectors to V_{NN} and save them in V_{NN}
  `// Find the antipodal partners and calculate the mean direction`
  Use algorithm A2 to generate the reduced vector list V_R containing n_R vectors
  `// For the fcc-lattice at least 6 neighbor directions need to be available`
  if $n_R < 6$ **then**
    return not oriented
  end
  `// Calculate three` $\langle 100 \rangle$ `directions`
  Empty $\langle 100 \rangle$-vector list V_{100}
  for $i = 0$; $i < n_R$; $i{+}{+}$ **do**
    $\vec{v_i}$ is the ith vector in V_R
    if *the number of vectors inside V_{100} is three* **then**
      break
    end
    `// check all` $ij = ji$ `combinations`
    for $j = i + 1$; $j < n_R$; $j{+}{+}$ **do**
      $\vec{v_j}$ is the jth vector in V_R
      if *the angle between $\vec{v_i}$ and $\vec{v_j}$ is in the interval $90^\circ \pm \Delta\beta$* **then**
        `// Calculate the crossproduct of` $\vec{v_i}$ `with` $\vec{v_j}$
        $\vec{v_{CP}} = \vec{v_i} \times \vec{v_j}$
        Append $\vec{v_{CP}}$ to V_{100}
        if *the number of vectors inside V_{100} is three* **then**
          break
        end
      end
    end
  end
  if *the number of vectors inside V_{100} is smaller than three* **then**
    return not oriented
  end
  Setup the matrix M as shown in equation (3)
  Calculate the orientation quaternion q as a least square solution to M, utilizing a 4×4-Matrix and computing the corresponding eigenvectors with Armadillo
  return the orientation id to q
end

Result: *The orientation id to the atoms orientation*

Algorithm A2: Algorithm reducing a nearest neigbor vector list by eliminating twice occurrences of antipodal vectors.

Input:

Vector list V_{NN} containing n_{NN} nearest neighbor unit-vectors of an atom

The antipodal threshold angle $\Delta\alpha$

Empty reduced-vector list V_R

for $i = 0$; $i < n_{NN}$; $i{+}{+}$ **do**

  v_i is the ith vector in V_{NN}

  `// check all` $ij = ji$ `combinations`

  for $j = i + 1$; $j < n_{NN}$; $j{+}{+}$ **do**

    v_j is the jth vector in V_{NN}

    if *both v_i and v_j are unpaired* **then**

      if *the angle between v_i and v_j is in the interval* $180° \pm \Delta\alpha$ **then**

        Append $\frac{1}{2}(v_i - v_j)$ to V_R

        v_i and v_j are marked as paired

      end

    end

  end

  `// Poor` v_i `didn't find a partner ?`

  if v_i *is still unpaired* **then**

    Append v_i to V_R

  end

end

Result: *The reduced vector list V_R*

Appendix A.2. Grain identification and reconstruction

In order to group atoms together into a grain entity, two different criteria were introduced. A *local criterion* that compares the orientation of a candidate atom i.e. that of the atom to be assigned to a certain grain and that of the reference atom, referred to as parent atom. A *global criterion* compares the average orientation of the grain and the orientation of the candidate atom.

Algorithm A3: Grain-identification algorithm grouping areas of similarly oriented atoms into grain entities.

```
Data: Position data for all atoms
Result: A certain number of grains
foreach atom a do
    if a has been assigned to any grain then
        continue
    end
    new grain G
    empty atom list l_N
    empty atom list l_NN
    add a to l_N with a as parent atom
    while number of entries of l_N > 0 do
        foreach atom a_n in l_N do
            if a_n has been assigned to any grain then
                continue
            end
            // local criterion
            if a_n and its parent atom have not a very close orientation then
                continue
            end
            // global criterion
            if the orientation of a_n and the average orientation of G are not close
            then
                continue
            end
            assign a_n to G
            add all nearest neighbors of a_n to l_NN with a_n as parent atom
        end
        l_N = l_NN
        l_NN = new empty list
    end
    if G does not comprise a sufficient amount of atoms then
        dissociate all atoms of G
        delete G
    end
end
```

Appendix A.3. Orphan atom adoption

The atoms that were not successfully assigned to a grain by the previous algorithm are referred to as *orphan atoms*. The current algorithm is used to assign these atoms to a grain in a procedure deemed as atom adoption, which is based on the most frequent occurrences of the same grain. A threshold for the minimum number of occurrences of a grain was implemented to suppress a random pick behavior. The procedure is repeated for every atom until no further adoptions can occur in the dataset.

Algorithm A4: Algorithm assigning atoms to preexisting grains by taking into account the grain-membership of nearest neighbor atoms.

Data: *Position data for all atoms*

Result: *A certain number of grains*

foreach *orphan atom* a_{orph} **do**
    count(all grains) = 0
    if a_{orph} *has been adopted by any grain* **then**
        continue
    end
    foreach *neighbor atom* a_n *to* a_{orph} **do**
        if a_n *is assigned to any grain* **then**
            count(grain(a_n)) ++
        end
    end
    identify the grain g_{MF} with the highest count c_{MF}
    if $c_{MF} \geq$ *minimum number of grain occurrence* **then**
        adopt a_n by g_{MF}
        // a_n is now assigned to g_{MF}
    end
end

Appendix A.4. Grain tracking over time

Algorithm A5 finds a corresponding grain-entity from a previously analyzed data set. Both the center-of-mass (COM) and the orientation of the grains are utilized as criteria to match couples from the data sets.

Algorithm A5: Algorithm assigning a currently detected grain to a grain-entity from a previous timestep.

Input: *a newly identified grain g*
Data:
Volume V_G of the grain g
some factor a
mapped grain g_{mapped} grain id $id_G = NO_GRAIN$
$d_{max} = a\left(\frac{V_G}{4/3\pi}\right)^{1/3}$
$d_{min} = d_{max}$
foreach *Grain g_{prev} from the previous timestep* **do**
    if *g_{prev} is already assigned to any grain* **then**
        continue
    end
    `// Center-of-mass distance-criterion`
    d = distance between COM(g) and COM(g_{prev})
    if $d > d_{max}$ **then**
        continue
    end
    `// Misorientation-criterion`
    $\Delta\varphi$ = misorientation between the average orientations of g and g_{prev}
    if $\Delta\varphi > \Delta\varphi_{max}$ **then**
        continue
    end
    `// All criteria fulfilled`
    if $d \leq d_{min}$ **then**
        $d_{min} = d$
        $g_{mapped} = g_{prev}$
        $id_G = id(g_{prev})$
    end
end
if $id_G \neq$ NO_GRAIN **then**
    `// do not allow a double assignment`
    set g_{mapped} as assigned
    return id_G
end
return a new id

Appendix A.5. Rotation quaternions and unique orientations

During the determination of the per-atom orientation, owing to the symmetry of the cubic lattice different but equivalent orientation quaternions may be calculated. For this reason, it is necessary to reduce the orientation to a unique one. This done by algorithm A6 by the utilization of Eqs. (A.1)-(A.24):

Algorithm A6: Algorithm to obtain the unique cubical orientation quaternion q_{uo} to a quaternion q.

Input: *An orientation quaternion q*

Cosine Angle $C_{max} = 0$
The unique quaternion to identify q_u
foreach *24 cubically equivalent quaternions* q_i *to* q **do**
    if $|q_i[0]| > C_{max}$ **then**
        $C_{max} = |q_i[0]|$
        $q_u = q_i$
    end
end
if $q_u[0] < 0$ **then**
    $q_u = -q_u$
end
return q_u

List of the 24 cubically-equivalent orientation quaternions:

$$q_1^T = [a_0; a_1, a_2, a_3] \tag{A.1}$$

$$q_2^T = [-a_1; a_0, a_3, -a_2] \tag{A.2}$$

$$q_3^T = [-a_2; -a_3, a_0, a_1] \tag{A.3}$$

$$q_4^T = [-a_3; a_2, -a_1, a_0] \tag{A.4}$$

$$q_5^T = 0.5[a_0 - a_1 - a_2 - a_3; a_0 + a_1 + a_2 - a_3, a_0 - a_1 + a_2 + a_3, a_0 + a_1 - a_2 + a_3] \tag{A.5}$$

$$q_6^T = 0.5[a_0 + a_1 + a_2 + a_3; -a_0 + a_1 - a_2 + a_3, -a_0 + a_1 + a_2 - a_3, -a_0 - a_1 + a_2 + a_3] \tag{A.6}$$

$$q_7^T = 0.5[a_0 - a_1 + a_2 - a_3; a_0 + a_1 + a_2 + a_3, -a_0 - a_1 + a_2 + a_3, a_0 - a_1 - a_2 + a_3] \tag{A.7}$$

$$q_8^T = 0.5[a_0 + a_1 - a_2 + a_3; -a_0 + a_1 - a_2 - a_3, a_0 + a_1 + a_2 - a_3, -a_0 + a_1 + a_2 + a_3] \tag{A.8}$$

$$q_9^T = 0.5[a_0 + a_1 - a_2 - a_3; -a_0 + a_1 + a_2 - a_3, a_0 - a_1 + a_2 - a_3, a_0 + a_1 + a_2 + a_3] \tag{A.9}$$

$$q_{10}^T = 0.5[a_0 - a_1 + a_2 + a_3; a_0 + a_1 - a_2 + a_3, -a_0 + a_1 + a_2 + a_3, -a_0 - a_1 - a_2 + a_3] \tag{A.10}$$

$$q_{11}^T = 0.5[a_0 + a_1 + a_2 - a_3; -a_0 + a_1 + a_2 + a_3, -a_0 - a_1 + a_2 - a_3, a_0 - a_1 + a_2 + a_3] \tag{A.11}$$

$$q_{12}^T = 0.5[a_0 - a_1 - a_2 + a_3; a_0 + a_1 - a_2 - a_3, a_0 + a_1 + a_2 + a_3, -a_0 + a_1 - a_2 + a_3] \tag{A.12}$$

$$q_{13}^T = \frac{1}{\sqrt{2}}[a_0 - a_1; a_0 + a_1, a_2 + a_3, -a_2 + a_3] \tag{A.13}$$

$$q_{14}^T = \frac{1}{\sqrt{2}}[a_0 - a_2; a_1 - a_3, a_0 + a_2, a_1 + a_3] \tag{A.14}$$

$$q_{15}^T = \frac{1}{\sqrt{2}}[a_0 - a_3; a_1 + a_2, -a_1 + a_2, a_0 + a_3] \tag{A.15}$$

$$q_{16}^T = \frac{1}{\sqrt{2}}[-a_1 - a_2; a_0 - a_3, a_0 + a_3, a_1 - a_2] \tag{A.16}$$

$$q_{17}^T = \frac{1}{\sqrt{2}}[-a_2 - a_3; a_2 - a_3, a_0 - a_1, a_0 + a_1] \tag{A.17}$$

$$q_{18}^T = \frac{1}{\sqrt{2}}[-a_1 - a_3; a_0 + a_2, -a_1 + a_3, a_0 - a_2] \tag{A.18}$$

$$q_{19}^T = \frac{1}{\sqrt{2}}[a_0 + a_1; -a_0 + a_1, a_2 - a_3, a_2 + a_3] \tag{A.19}$$

$$q_{20}^T = \frac{1}{\sqrt{2}}[a_0 + a_2; a_1 + a_3, -a_0 + a_2, -a_1 + a_3] \tag{A.20}$$

$$q_{21}^T = \frac{1}{\sqrt{2}}[a_0 + a_3; a_1 - a_2, a_1 + a_2, -a_0 + a_3] \tag{A.21}$$

$$q_{22}^T = \frac{1}{\sqrt{2}}[a_1 - a_2; -a_0 - a_3, a_0 - a_3, a_1 + a_2] \tag{A.22}$$

$$q_{23}^T = \frac{1}{\sqrt{2}}[a_2 - a_3; a_2 + a_3, -a_0 - a_1, a_0 - a_1] \tag{A.23}$$

$$q_{24}^T = \frac{1}{\sqrt{2}}[a_1 - a_3; -a_0 + a_2, -a_1 - a_3, a_0 + a_2] \tag{A.24}$$